Structure of zinc and niobium tellurite glasses by neutron and x-ray diffraction

2004 J. Phys.: Condens. Matter 16 1645

(http://iopscience.iop.org/0953-8984/16/9/013)

INSTITUTE OF PHYSICS PUBLISHING JOURNAL OF PHYSICS: CONDENSED MATTER

J. Phys.: Condens. Matter **16** (2004) 1645–1663 PII: S0953-8984(04)73316-0

Structure of zinc and niobium tellurite glasses by neutron and x-ray diffraction*

U Hoppe[1], E Yousef[2,3], C Rüssel[3], J Neuefeind[4,5] and A C Hannon[6]

[1] Department of Physics, Rostock University, Rostock D-18051, Germany
[2] Department of Physics, Al-Azhar University, Assiut Branch, Egypt
[3] Otto Schott Institute for Glass Chemistry, Friedrich Schiller University Jena, Jena D-07743, Germany
[4] Hamburger Synchrotronstrahlungslabor (HASYLAB) am Deutschen Elektronen-Synchrotron (DESY), Notkestraße 85, Hamburg D-22607, Germany
[5] Chemistry Division, Argonne National Laboratory, 9700 S Cass Avenue, Argonne, IL 60439, USA
[6] ISIS Facility, Rutherford Appleton Laboratory, Chilton, Didcot OX11 0QX, UK

Received 11 December 2003
Published 20 February 2004
Online at stacks.iop.org/JPhysCM/16/1645 (DOI: 10.1088/0953-8984/16/9/013)

Abstract

Neutron and x-ray diffraction experiments of high resolving power with neutrons from a spallation source and high-energy photons from a synchrotron have been performed on compositional series of binary Zn, Nb and on mixed Zn/Nb tellurite glasses. The Te–O, Zn–O and Nb–O coordination numbers are determined by Gaussian fitting of the first-neighbour peaks in the neutron and x-ray data simultaneously. The transition of TeO_4 to TeO_3 units with increasing fraction of a second component is indicated by decreasing total Te–O coordination numbers. This transition appears different for glasses with ZnO or Nb_2O_5 additions. Details of the Te–O peaks suggest there are two species of Te–O bonds with lengths of ∼0.19 and ∼0.21 nm. The change of their fractions shows excellent agreement with the existence of TeO_4 trigonal bipyramids and TeO_3 trigonal pyramids. All oxygen atoms from ZnO and Nb_2O_5 are used for rupture of Te–O–Te bridges, which is accompanied with a change of nearly all participating TeO_4 to TeO_3 groups. The tendency for a $TeO_4 \rightarrow TeO_3$ change decreases for glasses of higher second component content which is accompanied by the occurrence of TeO_4 groups with non-bridging oxygens. The Nb tellurite glasses show transition to network-forming behaviour with the formation of Nb–O–Nb bridges. The fractions of TeO_3 units of ternary Zn/Nb tellurite glasses agree with an additivity behaviour of the modifying effects of ZnO and Nb_2O_5 additions.

* Some of these results have already been presented in thesis work: Yousef E 2003 A study of some physical properties of tellurite glass (Al-Azhar University, Assiut Egypt).

1. Introduction

Interest in the structure of TeO_2-based glasses is mainly due to applications of related materials in lasers and non-linear optics devices. High refractive index, high third-order non-linear susceptibility, low phonon maxima and low melting point are the outstanding properties of these materials [1–6]. The primary structural units of such materials are assumed to be TeO_4 trigonal bipyramids and TeO_3 trigonal pyramids where a change from TeO_4 to TeO_3 groups occurs with increasing content of modifying oxide [7, 8]. Results of Raman and x-ray photoelectron spectroscopy [9], as well as of ^{125}Te nuclear magnetic resonance (NMR) [10–12] are analysed quantitatively. Fractions of groups in structures of binary tellurite glasses modified with mono-, bi- and some tri-valent metal atoms change uniformly. An oxygen atom introduced into glasses with high TeO_2 content opens a Te–O–Te bridge and changes two TeO_4 into TeO_3 units. Each of these TeO_3 units has two terminal Te–O bonds with partial double bond character. In contrast, only a small fraction of the oxygen introduced with V_2O_5 additions is used to modify the tellurite network (^{125}Te NMR [13]). The present scattering study is focused on Zn tellurite glasses of 'normal' modifying effect and a series of Nb tellurite glasses of unknown behaviour. A few mixed Zn/Nb tellurite glasses are also included. ZnO and Nb_2O_5 are important additives in manufacturing host materials for fibre amplifiers [5, 6].

Results of a series of V tellurite glasses which were obtained under the same experimental conditions have been published [14]. Use of neutrons from spallation sources allows scattering data to be obtained up to a high magnitude of momentum transfer Q of 400 nm^{-1} ($Q = 4\pi/\lambda \sin\theta$ with λ the radiation wavelength and 2θ the scattering angle). Due to this Q_{max} details of the Te–O distances can be resolved [14]. V–O distances are negligible because the neutron scattering length of V atoms is very small. Similar experiments ($Q_{max} = \sim 300$ nm^{-1}) have been made on Ba, Na and Li tellurite glasses [15–17]. Ba samples have the advantage of large Ba–O separations which do not interfere with the Te–O first-neighbour distances. However, oxygen neighbours of Zn and Nb are expected to lie at similar distances as the lengths of the Te–O bonds. To avoid making assumptions about Zn–O and Nb–O distances a second diffraction experiment with different contrast is needed. Nb and Zn are good scatterers for neutrons, little better than Te, but have fewer electrons for scattering of x-rays. The change of contrast between neutron and x-ray scattering data should be sufficient to resolve the Te–O and Zn–O (Nb–O) first-neighbour distances.

Excellent resolving power due to the high Q_{max} allows determination of fractions of short and long Te–O bonds which can be related to geometrical specifics of the TeO_4 and TeO_3 units. Examples of the structural units are shown in figure 1 where the bond lengths given are taken from structural groups of related crystals TeO_2 [18–20], $Nb_2Te_3O_{11}$ [21] and $Nb_2Te_4O_{13}$ [22]. The lone pair ($5s^2$ electrons) of a $Te_{(IV)}$ atom forces all oxygen atoms bonded to the Te toward positions on the opposite side of a plane which extends perpendicular to the line Te atom–lone pair and through the Te position. Lone pair and oxygen neighbours of the TeO_3 and TeO_4 units form trigonal pyramids (tp) and trigonal bipyramids (tbp) respectively, which are also illustrated in figure 1. Most Te–O bonds have lengths of $\sim$0.19 nm but greater Te–O distances of $\sim$0.21 nm exist with the oxygens in axial positions of the TeO_4 units. This differentiation of bond lengths is independent of the number of non-bridging oxygens (NBO) in these groups (see, for example, the TeO_4 units of various crystals shown in figure 1). The variety of groups found in crystals is greater than the two species mentioned. TeO_{3+1} units are known in $Nb_2Te_4O_{13}$ [22] and $Zn_2Te_3O_8$ [23]. Here two TeO_{3+1} share a common edge (figure 1). TeO_{3+2} groups exist in the $Cs_2Te_4O_9$ crystal [24]. One or two additional bonds are clearly longer than the other three. Some authors assume the existence of TeO_3 and TeO_4 units as being sufficient to describe the structural evolution of modified tellurite glasses [9–14]. In addition, the existence of TeO_{3+1}

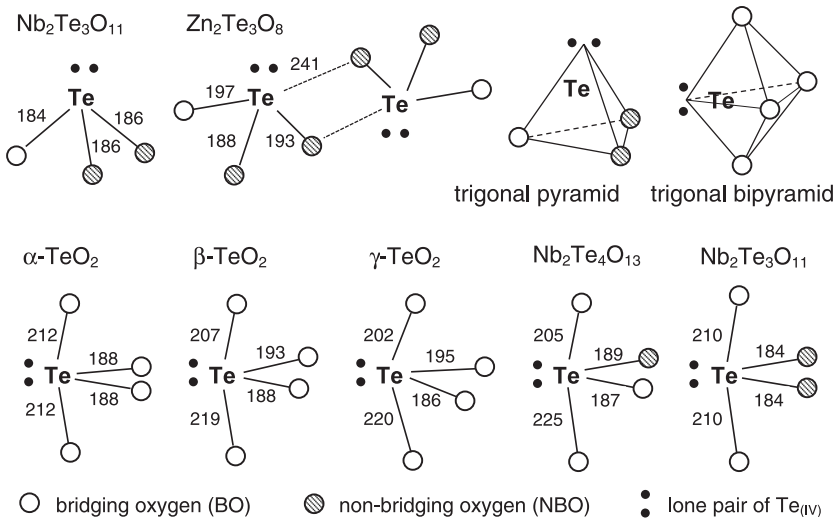

Figure 1. Basic TeO_n building groups of related tellurite crystals. Upper part: TeO_3 units in $Nb_2Te_3O_{11}$ [21] and TeO_{3+1} units in $Zn_2Te_3O_8$ [23] crystals. Lower part: TeO_4 units with different numbers of NBO in α-TeO_2 [18], β-TeO_2 [19], γ-TeO_2 [20], $Nb_2Te_4O_{13}$ [22] and $Nb_2Te_3O_{11}$ [21] crystals. Bond lengths are given in picometres. In the upper right, polyhedra of lone pair and oxygen neighbours are illustrated as trigonal pyramids (TeO_3) and trigonal bipyramids (TeO_4).

units in glass structures is suggested on the basis of Raman spectra [25–28] and diffraction data [16, 25]. However, it is argued [17, 25] that differences between the indications for TeO_3 or TeO_{3+1} units are small. The present diffraction experiments of high resolving power should contribute to clarification of this problem.

2. Experimental details

Glasses were prepared by mixing appropriate amounts of the oxides TeO_2 99.999% purity (Ferak), Nb_2O_5 99.5% purity (Fluka AG) and ZnO 99.5% purity (Chemapol). The mixed powders were melted in gold crucibles in a furnace at temperatures from 1023 to 1123 K for 30 min. The melts were cast at 1023 K in graphite moulds which were set to an annealing furnace at 600 K for 2 h. The samples were cooled to room temperature by switching off the furnace. Visibly homogeneous glasses of a light yellow colour are formed. The sample compositions, the labels subsequently used and their mass densities as measured with a helium pycnometer are given in table 1.

The neutron diffraction experiments were performed at the GEM diffractometer of the ISIS spallation source of the Rutherford Appleton Laboratory (Chilton, UK). The glassy material was crushed and loaded into 8.3 mm diameter vanadium cylinders with a wall thickness of only 0.025 mm. The beam size was 12×40 mm^2. The duration of the data collection was a minimum of 3 h for each sample. A 6 mm vanadium rod was used to obtain the incident energy spectrum which is needed for data normalization in the time-of-flight regime. The diffraction data were corrected using standard procedures for container and background scattering, attenuation, multiple scattering and inelasticity effects [29]. For technical reasons only the differential scattering cross-sections, $d\sigma/d\Omega$, collected in the detector groups 2 (scattering angles 14°–21°) and 5 (79–104°) could be used. The resulting functions of sample znt22 are shown in figure 2. The unusual decays of intensities for $Q > 80$ and 400 nm^{-1} respectively are due to effects of a

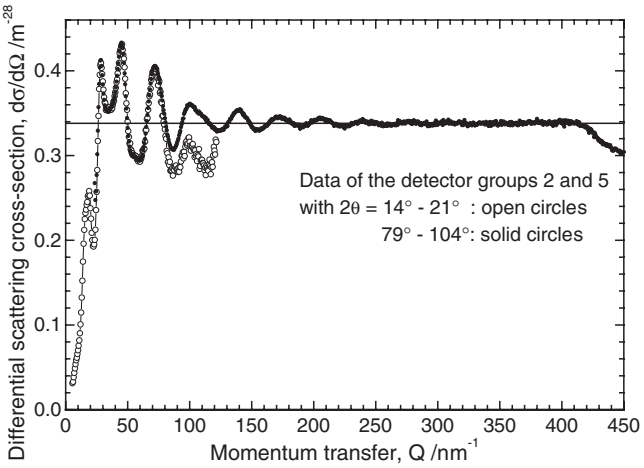

Figure 2. Differential scattering cross sections, $d\sigma/d\Omega$, obtained by neutron diffraction of sample znt22. The data given for two detector groups of the GEM instrument were obtained after finishing all corrections and normalization. They are used to calculate the final structure factor.

Table 1. Compositions and densities of the tellurite glasses studied.

Sample label	Molar fractions c_i			$c(M_yO)$	Mass density (g cm^{-3})	Number density of atoms (nm^{-3})
	ZnO	Nb_2O_5	TeO_2			
znt22	0.22	—	0.78	0.220	5.520(2)	64.9
znt30	0.30	—	0.70	0.300	5.485(2)	65.6
nbt06	—	0.06	0.94	0.242	5.539(2)	65.1
nbt10	—	0.10	0.90	0.357	5.508(2)	66.3
nbt18	—	0.18	0.82	0.523	5.378(2)	67.4
nzt05	0.05	0.05	0.90	0.250	5.479(2)	64.6
nzt20	0.20	0.05	0.75	0.375	5.401(2)	67.1
nzt12	0.125	0.10	0.775	0.446	5.375(2)	67.5

resonance of Te nuclei for epithermal neutrons of 2.3 eV. For composing the final Faber–Ziman structure factors $S_N(Q)$ [30] the data for group 2 were adjusted to the data for group 5. A significant but small continual increase of the data for $Q < 100\ \text{nm}^{-1}$ might be due to deficits of inelasticity corrections for neutrons of wavelengths greater than 0.1 nm. The increase was empirically removed whereby the minimization of unphysical oscillations in the correlation functions, $T(r)$ (cf figure 5), for distances r smaller than the position of the peak of shortest bonds, was the criterion. Changes to the first-neighbour peaks due to this modification of data are not significant.

The x-ray diffraction experiments were performed at the BW5 wiggler beamline at DORIS III of the Deutsches Elektronen-Synchrotron (Hamburg). An incident photon energy of 120 keV ($\lambda = 0.0104$ nm) was chosen for the experiments. The beam size was $1 \times 4\ \text{mm}^2$. Exact absorption corrections are difficult because the 1.5 mm diameter of of the silica capillaries (with wall thickness of 0.01 mm) containing the glassy powder exceeds the beam width. The scattering angles are small ($2\theta = 28°$ for $Q_{\max} = 300\ \text{nm}^{-1}$) and the transmission coefficients are greater than 0.9 so that absorption is independent of the angle θ. The electronic energy window of the solid state Ge detector was chosen to pass the elastic line and the full Compton peak but no fluorescence radiation. Dead-time corrections were made

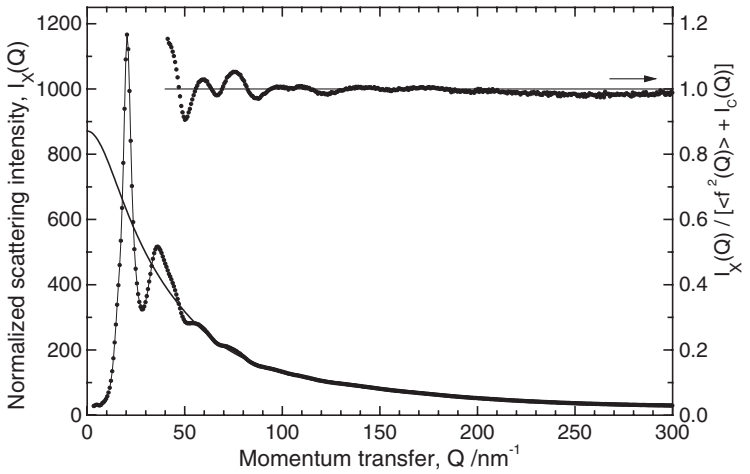

Figure 3. X-ray scattering intensities, $I_X(Q)$, of sample znt22 after finishing all corrections and normalization. The solid-curved function is the structure-independent scattering which is the sum of the compositional average of the square of atomic scattering amplitudes $\langle f^2(Q)\rangle$ and of the Compton scattering $I_C(Q)$. The quotient of both functions is shown in the upper right to make visible small normalization deficits in the high-Q range.

with the parameter $\tau = 1.08\ \mu$s [31] and a fraction of 0.91 of incident photons is polarized horizontally. Corrections were made for background, container scattering, polarization and absorption. Subsequently, scattering intensities were normalized to structure-independent scattering functions which were calculated by a polynomial approach [32] of tabulated atomic data of the elastic scattering factors [33] where the fraction of Compton scattering is calculated according to [34]. Figure 3 shows the scattering intensities of sample znt22 after normalization together with the structure-independent scattering. A quotient of both functions is shown in the upper-right section of the figure. The quality of data is sufficient to make an excellent normalization. An empirical correction with a smooth function was used in the range of $Q \gtrsim 200\ \text{nm}^{-1}$ that makes the scattering intensity oscillate around the structure-independent scattering. As well as deficits in the calculation of the Compton fraction, uncertainties in the chemical compositions, errors in the instrument calibration, instabilities of beam position and monitor efficiencies can also cause deviations. Finally, the Faber–Ziman structure factors, $S_X(Q)$, are calculated [30, 35].

3. Results

3.1. Structure factors and correlation functions

The neutron and x-ray structure factors shown in figures 4(a) and (b) are weighted with Q to make visible the oscillations in the high-Q range. Although from sample to sample systematic changes of the $S(Q)$ data are only visible for $Q < 50\ \text{nm}^{-1}$ measurement of the high-Q range is very important. Subtle changes in that range indicate changes in the short-range order which only become visible after analysis of the first-neighbour peaks in real space. Data for high Q-values are important to obtain a maximum of detailed information about these peaks by reducing the truncation effects of Fourier transformation (FT). Use of thin-walled containers helps to minimize normalization errors, which is important for combination of neutron and

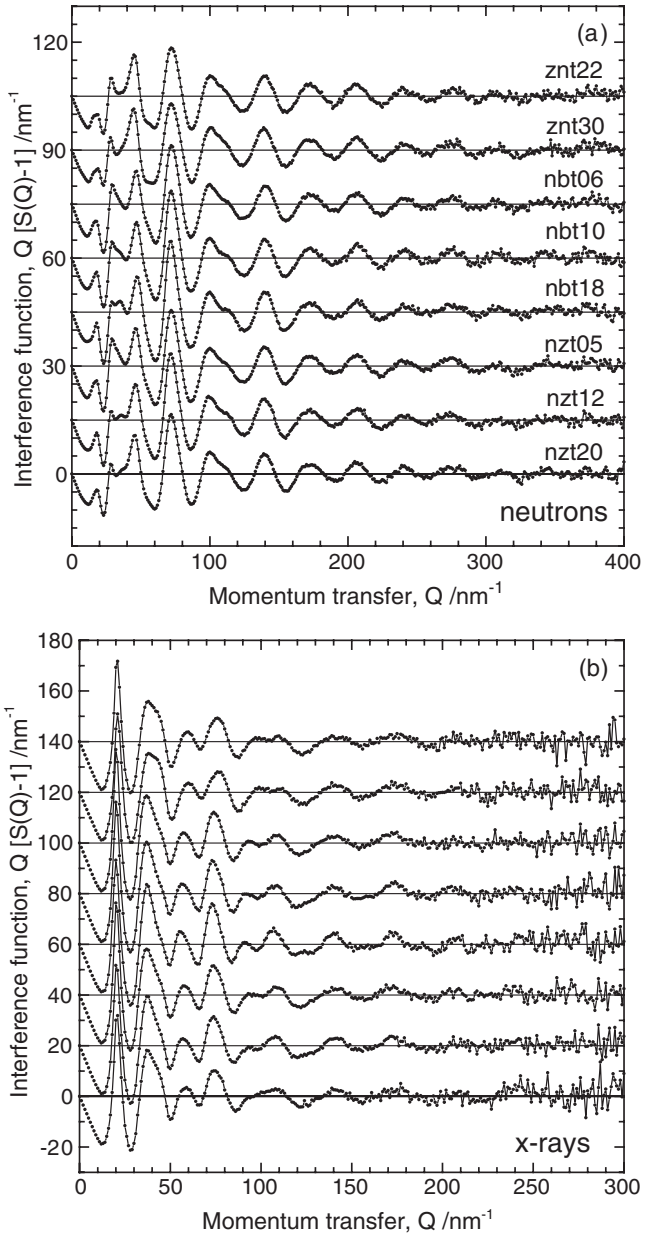

Figure 4. Weighted structure factors of the samples studied: (a) neutron data and (b) x-ray data. Upper functions are shifted for clarity.

x-ray data. The correlation functions, $T(r)$, are calculated by FT with

$$T(r) = 4\pi r\rho_0 + 2/\pi \int_0^{Q_{\max}} Q[S(Q) - 1]M(Q)\sin(Qr)\,\mathrm{d}Q. \tag{1}$$

Here ρ_0 is the number density of atoms (table 1). The function $M(Q)$ is introduced for damping of spurious features such as ripples caused by noise and by termination of the Fourier integral at $Q_{\max}$. A function $M(Q) = \sin(\pi Q/Q_{\max})/(\pi Q/Q_{\max})$ [36] is used. The $T(r)$ functions

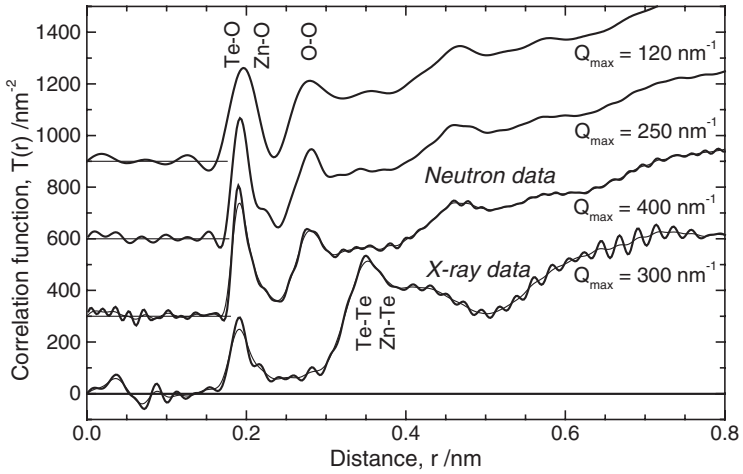

Figure 5. Comparison of neutron and x-ray correlation functions, $T_N(r)$ and $T_X(r)$, of the sample znt22 obtained with damping (thin solid curves) and without damping (thick solid curves) [36]. The Q_{max} used in the Fourier transformation are given in the plot. Two $T_N(r)$ functions obtained with reduced Q_{max} illustrate the truncation effect. Upper functions are shifted for clarity.

for sample znt22 obtained with and without applying $M(Q)$ are compared in figure 5. For the neutron $T_N(r)$ functions obtained with $Q_{max} = 400\ nm^{-1}$ only a difference in the width of the Te–O peak component at ∼0.19 nm is detected. Broadening of distance peaks caused by this Q_{max} is already a weak effect. The broadening with fwhm of 0.0095 nm ($3.791/Q_{max}$ [37]) is smaller than the peak widths of the glass structure which are obtained by Gaussian fitting. Thus, the neutron $T_N(r)$ function with $Q_{max} = 400\ nm^{-1}$ exhibits almost all details which can be extracted; the termination oscillations are also small. Hence, $T_N(r)$ functions obtained without damping are used in the subsequent fits. In case of the x-ray $T_X(r)$ functions a similar difference of widths exists for the peak at ∼0.19 nm (figure 5), but other clear oscillations also exist in the $T_X(r)$ data obtained without damping. Their origin is not clear. They could be due to termination effects, but also to the noise in the high-Q data. Therefore, this function is not used in the fits; we use the $T_X(r)$ obtained with damping ($Q_{max} = 300\ nm^{-1}$). The origin of some unphysical oscillations of this function at ∼0.05 nm was not identified. To emphasize the importance of a large measuring range, figure 5 also shows the $T_N(r)$ functions obtained with smaller Q_{max}. That function with $Q_{max} = 250\ nm^{-1}$ has a shoulder at $r = \sim 0.22$ nm which appears enhanced from termination effects and does not reflect a real distance peak. The function with $Q_{max} = 120\ nm^{-1}$ does not resolve any asymmetry of the Te–O peak.

3.2. Gaussian fitting of the first-neighbour peaks

Sharp Te–O peaks are found at 0.19 nm which are accompanied by tails extending to 0.24 nm. The Zn–O and Nb–O contributions expected at 0.20 nm are not resolved as separate peaks (cf figures 6(a) and (b)). They are only visible as weak shoulders in $T_N(r)$. A possible approach to resolving the Te–O, Zn–O and Nb–O distances is the calculation of a difference of $S_X(Q)$ and $S_N(Q)$ factors in analogy to isomorphic or isotopic substitution methods. On the other hand, we have a different quality of data in the range of high Q and do not want to lose structural information. Therefore, Gaussian fitting is performed with the $T_N(r)$ and $T_X(r)$ data simultaneously where definite series of Gaussian functions are used to approximate the pair correlations in the range of first-neighbour distances. The effects caused by termination of

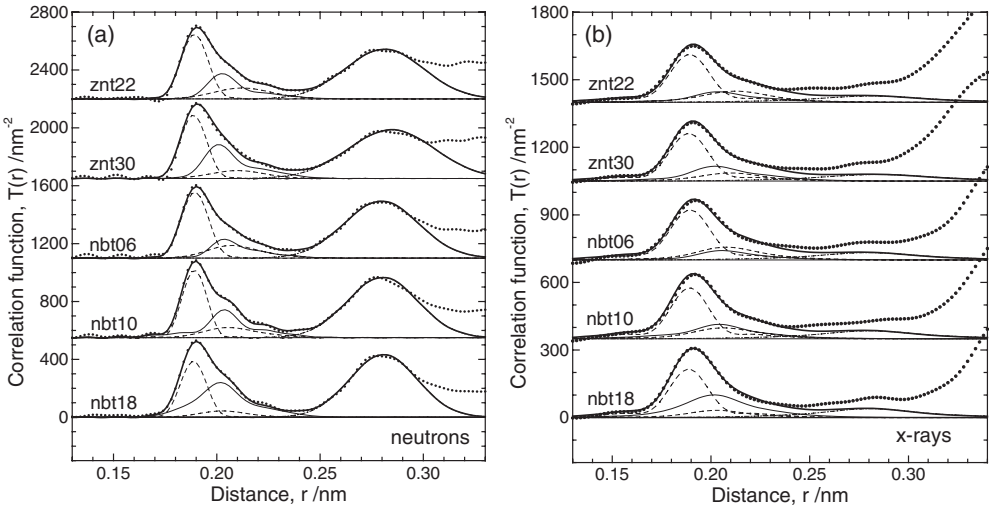

Figure 6. Correlation functions (dotted curves) of the binary Zn and Nb tellurite glasses studied: (a) neutron data obtained by FT with $Q_{\max} = 400$ nm^{-1} and (b) x-ray data obtained by FT with $Q_{\max} = 300$ nm^{-1} and damping [36]. The model $T(r)$ functions are given as thick solid curves, the partial correlations are given as dashed curves (Te–O), thin solid curves (Zn–O or Nb–O) and dash–dotted curves (O–O).

FT at $Q_{\max}$ are taken into account by convolution of the model Gaussian functions with peak functions, $P_{ij}(r)$, which simulate the Q window and damping used in equation (1) [37–39]. The parameters are the coordination numbers N_{ij}, the mean distances r_{ij}, and the peak widths (full widths at half maximum) Δr_{ij}. Least-squares fits are performed using the Marquardt algorithm [40]. The constraints and parameters fixed in the fits have been varied several times to find the appropriate number of Gaussian functions that are needed to approximate the experimental correlation functions. Starting parameters are taken from earlier work and from related crystal structures, as detailed in the subsequent sections.

The Te–O peak component is approximated by three Gaussian functions as this was successful for V tellurite glasses where the role of V–O correlations is negligible in $T_{\mathrm{N}}(r)$ [14]. The Zn–O correlations of the glass samples znt22 and znt30 are formed by two Gaussian functions, as used for Zn phosphate [41] and Zn vanadate glasses [42]. The two functions form a peak at ∼0.205 nm with a flat tail of greater distances, as happens with Zn tellurite crystals [23, 43] where the Zn–O coordination number, N_{ZnO}, is 6 or 5. The model O–O peak is a single Gaussian which may include small Te–O or Zn–O contributions exceeding distances of 0.24 nm. The height of this peak is chosen to fit the O–O peak in the $T_{\mathrm{N}}(r)$ functions (figure 6(a)). The $T_{\mathrm{X}}(r)$ data (figure 6(b)), however, are not well fitted in this r-range. Two correlation functions, $T_{\mathrm{N}}(r)$ and $T_{\mathrm{X}}(r)$, do not allow resolution of the three pair correlations of Te–O, Zn–O (Nb–O) and O–O pairs.

Not all parameters of the Te–O and Zn–O correlations are adjusted by the fits, but few of them have been fixed. These parameters are marked in table 2. Moreover, the third Te–O distance is set equal to the second Zn–O distance. Uncertainties are only given for total numbers N_{ij} and for distances of the first peak components. The other parameters are only relevant for properly fitting the shape of the pair correlations and do not possess specific physical meaning. The Te–O distances are split up into two components according to different bond lengths in the TeO_4 units (figure 1). The number N_{short} of short Te–O bonds is taken from the first narrow

Table 2. Parameters resulting from Gaussian fitting of the Te–O, Zn–O, Nb–O and O–O first-neighbour peaks of the binary glasses. Distances and full widths at half maximum (fwhm) are given in nanometres. Numbers in parenthesis give the uncertainty in the last digit.

Sample	Atom pair	Coordination number	Distance	fwhm	Total coordination number	N_{short}	N_{long}
znt22	Te–O	2.48	0.189(1)	0.015(2)	3.51(10)	2.48(10)	1.03(20)
		0.61	0.210[a]	0.030[a]			
		0.42	0.218	0.035[a]			
	Zn–O	3.09	0.202(2)	0.015(3)	5.2(3)		
		2.12	0.218	0.035[a]			
	O–O	6.90	0.281	0.045			
znt30	Te–O	2.55	0.189(1)	0.014(2)	3.28(10)	2.55(10)	0.73(20)
		0.70	0.210[a]	0.030[a]			
		0.03	0.216	0.035[a]			
	Zn–O	2.76	0.200(2)	0.015(2)	5.3(2)		
		2.52	0.216	0.035[a]			
	O–O	7.70	0.285	0.049			
nbt06	Te–O	2.51	0.189(1)	0.015(2)	3.58(10)	2.51(10)	1.07(20)
		0.63	0.205	0.025[a]			
		0.44	0.217	0.035[a]			
	Nb–O	1.07	0.202	0.008	7.2(4)		
		2.79	0.205	0.019			
		3.34	0.217	0.035[a]			
	O–O	7.23	0.280	0.042			
nbt10	Te–O	2.56	0.189(1)	0.013(2)	3.53(10)	2.56(10)	0.97(20)
		0.57	0.203	0.025[a]			
		0.40	0.217	0.035[a]			
	Nb–O	1.49	0.186	0.038	7.2(3)		
		2.73	0.203	0.012			
		2.97	0.217	0.035[a]			
	O–O	7.32	0.280	0.040			
nbt18	Te–O	2.75	0.189(1)	0.014(2)	3.39(10)	2.75(10)	0.64(20)
		0.53	0.202	0.025[a]			
		0.11	0.217	0.035[a]			
	Nb–O	1.46	0.189	0.024	6.55(20)		
		2.63	0.202	0.017			
		2.46	0.217	0.035[a]			
	O–O	7.40	0.281	0.039			

[a] These values are fixed in the fits.

Gaussian function while the number N_{long} of long Te–O bonds is the sum of the N_{ij} of the next two broader Gaussian functions. The corresponding Te–O peaks are shown as dashed-curved functions in figures 6(a) and (b). The numbers N_{ZnO} do not change for the samples znt22 and znt30 but the total number N_{TeO} decreases with increasing ZnO content, which is mainly due to a decrease in N_{long}.

The approach for fitting the data for Zn glasses used above was not successful with the data for the binary Nb tellurite glasses. Three instead of two Gaussian functions have to be used to approximate the Nb–O first-neighbour peaks. This behaviour becomes clear after inspecting

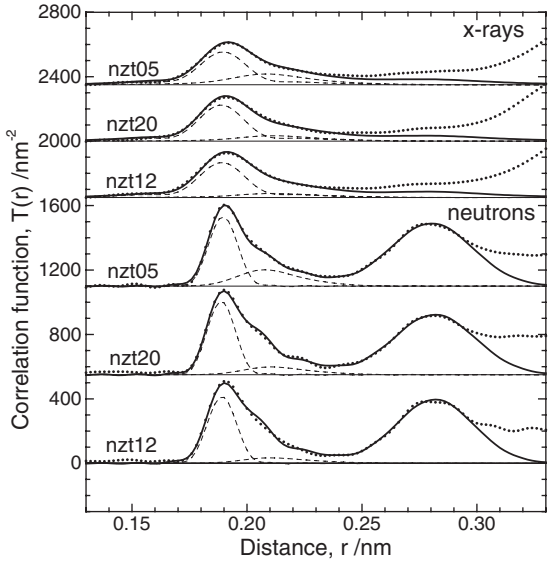

Figure 7. Correlation functions (dotted curves) of the ternary Zn/Nb tellurite glasses studied: (upper part) neutron data obtained by FT with $Q_{max} = 400$ nm^{-1} and (lower part) x-ray data obtained by FT with $Q_{max} = 300$ nm^{-1} and damping [36]. The model $T(r)$ functions are given as thick solid curves and the Te–O correlations are given as dashed curves.

Table 3. Parameters resulting from Gaussian fitting of the Te–O and O–O first-neighbour peaks of the ternary glasses. Distances and fwhm are given in nanometres. Numbers in parenthesis give the uncertainty in the last digit.

Sample	Atom pair	Coordination number	Distance	fwhm	Total coordination number	N_{short}	N_{long}
nzt05	Te–O	2.29	0.190(1)	0.014(2)	3.61(10)	2.29(10)	1.32(20)
		0.76	0.205	0.025[a]			
		0.56	0.220	0.035[a]			
	O–O	7.19	0.280	0.042			
nzt20	Te–O	2.69	0.189(1)	0.014(2)	3.44(10)	2.69(10)	0.75(20)
		0.42	0.208	0.025[a]			
		0.33	0.224	0.035[a]			
	O–O	7.06	0.282	0.042			
nzt12	Te–O	2.71	0.189(1)	0.014(2)	3.30(10)	2.71(10)	0.59(20)
		0.31	0.207	0.025[a]			
		0.28	0.224	0.035[a]			
	O–O	7.08	0.282	0.040			

[a] These values are fixed in the fits.

the distributions of Nb–O distances in $Nb_2Te_4O_{13}$ [22] and $Nb_2Te_3O_{11}$ [21] crystals: lengths from 0.18 to 0.22 nm are found in distorted NbO_6 octahedra. Here some peak widths are also fixed in the fits. Distances r_{ij} of the second and third Te–O and Nb–O Gaussian functions are set equal to each other (table 2). The final total numbers N_{NbO} vary from 6.5 to 7.2 which are greater than in the crystal structures with $N_{NbO} = 6$ [21, 22]. As already found for the Zn glasses, the total numbers N_{TeO} decrease with increasing content of second oxide. The numbers

N_{short} increase while the numbers N_{long} decrease. The final fits for the samples nbt06, nbt10 and nbt18 are also shown in figures 6(a) and (b). All parameters of the Gaussian functions are given in table 2.

Similar fits would lead to equivocal results for the ternary Zn/Nb tellurite glasses due to overlap of three different pair correlations in the range of the first-neighbour peak, while only two data sets, $T_N(r)$ and $T_X(r)$, of different contrast are available. Therefore, the parameters of the Zn–O and Nb–O correlations are taken from samples znt22, nbt10 and nbt18 and are fixed in the fits. The resulting parameters given in table 3 concern only the Te–O and O–O correlations. The corresponding $T_N(r)$ and $T_X(r)$ functions are given in figure 7 where, for clarity, the Zn–O and Nb–O contributions are not shown but only the peaks of short and long Te–O bonds (dashed curves). Here also sample nzt05 with the smallest modifier content shows the greatest total number N_{TeO} with the smallest fraction of short but greatest fraction of long Te–O bonds.

4. Discussion

4.1. Transition from TeO_4 to TeO_3 units with increasing fraction of second oxide

Unlike in the diffraction investigations of V tellurite glasses [14] or of Ba tellurite glasses [15] a combination of neutron and x-ray scattering is essential for determination of the Te–O distances of binary Zn or Nb tellurite glasses. A good fit of the $T_N(r)$ and $T_X(r)$ data was possible up to distances of 0.24 nm. The determination of fractions of Te–O and Zn–O (or Nb–O) distances in this range turns out to be almost independent of changes of details in the series of Gaussian functions used for fitting the relevant pair correlations. First, we assume distances less than ∼0.24 nm to be free of contributions from the longer bonds in possibly existing TeO_{3+1} units (cf figure 1). In this case, total Te–O coordination numbers yield the fractions of TeO_4 and TeO_3 units in the glass structure. The TeO_{3+1} units which possibly exist belong to the TeO_3 fraction. The corresponding results are plotted in figure 8, where the N_{TeO} numbers of V tellurite glasses [14] are also shown. The fractions of TeO_3 units, N_3, with $N_3 = 4 - N_{TeO}$ are given as a function of fractions $c(M_yO)$ which allow comparison of the modifying effect of metal oxides of Me of different valency. A similar diagram was given by Sakida *et al* [13] showing ^{125}Te NMR results. Figure 8(b) compares our diffraction results with the ^{125}Te NMR data [10, 12, 13]. The N_3 values of the Zn tellurite glasses are found to be close to the N_3 from ^{125}Te NMR of typical modifier oxides. Also the much smaller N_3 values of V tellurite glasses [14] are found to be close to the corresponding ^{125}Te NMR data [13]. (Results for a questionable 4 mol% V_2O_5 sample [14] are not shown.) The N_3-fractions of the binary Nb and mixed Zn/Nb tellurite glasses are between those of Zn and V tellurite glasses. The N_3 of the sample with the smallest Nb_2O_5 content (nbt06) tends to the behaviour of Zn tellurite glasses while the N_3 of the sample with the highest Nb_2O_5 content (nbt18) tends to the behaviour of V tellurite glasses.

Samples with very high TeO_2 content have not been measured in the present study. Since all other published data [7–13, 15–17, 25–28] solely support the existence of TeO_4 units in glasses with compositions approaching pure TeO_2 we follow the starting point of models developed earlier [9–12]: each oxygen atom of an added modifier oxide ruptures a Te–O–Te bridge forming two NBO and, in a second step, each of the two participating TeO_4 units with an NBO transforms to a TeO_3 unit with two NBOs. Note that one of the terminal bonds of the TeO_3 units is a double bond which delocalizes to both Te–NBO bonds according to resonance. Thus, an increase of the N_3 fraction with

$$N_3 = 2n(M_yO)/n(TeO_2) \tag{2}$$

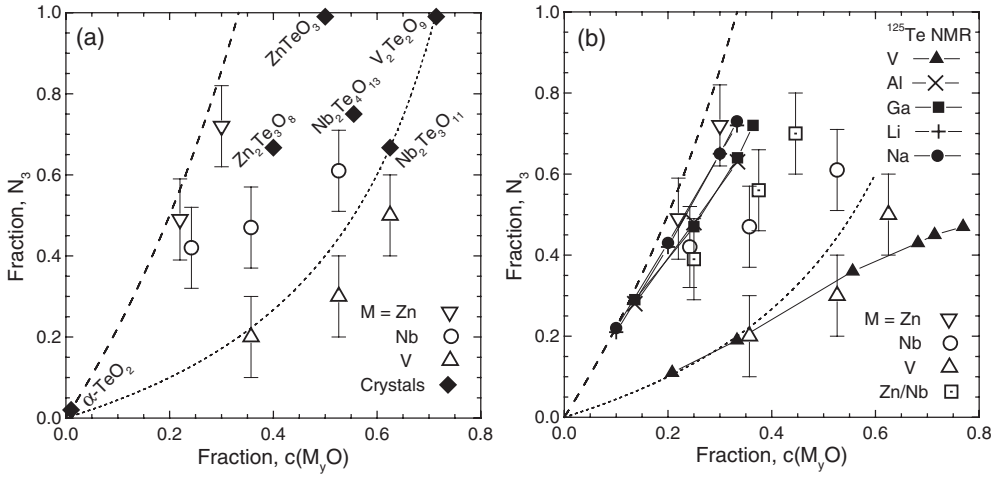

Figure 8. Fractions, N_3, of the TeO_3 units of the glasses studied versus fraction $c(M_yO)$ of modifier oxide. The N_3 values are calculated from total Te–O coordination numbers. Diffraction results are given with open symbols. Results for V tellurite glasses are taken from [14]. Data of related crystal structures are indicated with solid diamonds and their chemical formula (a). The ^{125}Te NMR results [10, 12, 13] are plotted as symbols connected by curves (b). The dashed- and dotted-curved functions give specific models of modifier behaviour which are explained in the text.

is expected (dashed curve in figure 8). Actually, this behaviour seems to be effective for all modifying oxides in the case of small M_yO additions. On the other hand, only ∼20% of the oxygen atoms of V_2O_5 in V tellurite glasses are used for such a transition [13, 14]. This behaviour is expressed by the dotted-curved function in figure 8. The greater fraction of the oxygen of V_2O_5 is retained in bonds with only V neighbours.

Raman [9] and ^{125}Te NMR [10–13] spectroscopy have shown that only in the range with $c(M_yO) \lesssim 0.2$ does each oxygen atom cause the process described by equation (2). Only the N_3 value of the glass with 22 mol% ZnO is found to be close to this behaviour. The other samples possess N_3 fractions which are less than predicted while the values of Nb glasses high in Nb_2O_5 content approach the behaviour calculated for V tellurite glasses. For glasses with higher $c(M_yO)$ fractions it has been shown [9, 12] that some of the TeO_4 units with NBO produced by rupture of Te–O–Te bridges do not change to TeO_3 units. The $TeO_4 \rightarrow TeO_3$ transition is even reduced for V tellurite glasses [13, 14] where, from the very beginning, the level of N_3 is only 20% of that of the other modified tellurite glasses. In the case of this glass series the N_3 value of the structure of the related $V_2Te_2O_9$ crystal [44] occupies the end point of the model $TeO_4 \rightarrow TeO_3$ change (dotted curve in figure 8). The fractions of N_3 of the glasses do not approach this high number but they retain a level of ∼0.5 for even the highest V_2O_5 content [13, 14].

It should be noted that the fractions of metal oxide of related Zn and Nb crystals [21–23, 43] are higher than those of the glasses studied. The N_3 fractions of these crystals do not obey the model behaviour of the $TeO_4 \rightarrow TeO_3$ change (equation (2)). TeO_4 units with two NBO exist in $Nb_2Te_3O_{11}$ [21] and $Zn_2Te_3O_8$ [23] crystals and TeO_4 units with one NBO are found in $Nb_2Te_4O_{13}$ [22] (cf figure 1). Moreover, both Nb tellurite crystals have oxygen atoms not connected to Te sites which are located in Nb–O–Nb bridges. The N_3-values of the Nb tellurite crystals show a larger deviation from the dashed-curved function in figure 8 than those of the Zn tellurite crystals and the N_3 fractions of the two Nb glasses of higher Nb_2O_5 content (nbt10,

nbt18) are approaching these N_3. Hence, an oxygen fraction of the Nb tellurite glasses high in Nb_2O_5 content is assumed to be in Nb–O–Nb bridges. The smaller difference from the model behaviour according to equation (2) of the N_3 value of the first sample (nbt06) is assumed to be due to the existence of TeO_4 units with NBO, a behaviour which also explains the small differences between the N_3 fractions of znt22 and znt30 samples and the model behaviour.

Another point gives support to the change of Nb from simple modifier behaviour (as found for Zn) to the development of network-forming properties. Nb–O–Nb bridges in the structure of $Nb_2Te_3O_{11}$ [21] and $Nb_2Te_4O_{13}$ [22] crystals possess Nb–O distances of ∼0.18 nm which are shorter than those in Nb–O–Te bridges. Three Gaussian functions have to be used for the Nb–O correlations when fitting the first-neighbour peaks for the Nb tellurite glasses. The short distance (∼0.18 nm) is not detected for the nbt06 sample. But, on average, 1.5 oxygen atoms were found at ∼0.188 nm for each Nb atom in the structures of nbt10 and nbt18 samples (table 2 and figure 3). Thus, the addition of Nb_2O_5 to tellurite glasses starts with network-modifying behaviour where some TeO_4 units with NBO already indicate a difference from the model behaviour (equation (2)). If the Nb_2O_5 content approaches ∼10 mol% some oxygens are found in Nb–O–Nb bridges, which indicates that Nb_2O_5 has a network-forming property.

4.2. Comparisons with the short-range order of related crystal structures

For the glasses znt30 and nbt18 with compositions close to those of $Zn_2Te_3O_8$ [23] and $Nb_2Te_4O_{13}$ [22] crystals, a comparison of the short-range structures might be useful. All Te–O, Zn–O (or Nb–O) distances of the crystal structures are assumed as Gaussian functions with widths chosen to be similar to those obtained from the fits (table 2). Widths of 0.013 nm, for example, are chosen for all short Te–O bonds. Parameters of the O–O peak are chosen to fit the peak at 0.28 nm in $T_N(r)$. For appropriate comparison with the experimental $T_N(r)$ and $T_X(r)$ data, the series of Gaussian functions of distances taken from the crystals are convoluted with peak shape functions $P_{ij}(t)$ [37–39], as introduced before. The results are shown in figure 9. The agreement of the short-range order of sample nbt18 with that of $Nb_2Te_4O_{13}$ [22] crystal is excellent except for a bump in $T_N(r)$ at ∼0.223 nm. This bump is attributed to additional oxygen neighbours of Nb atoms in the glass. N_{NbO} is 6 for the crystal while $N_{NbO} = 6.55$ was found for sample nbt18. More differences exist between the short-range structures of sample znt30 and the $Zn_2Te_3O_8$ [23] crystal. The first peaks of the $T_N(r)$ and $T_X(r)$ functions of the crystal structure are too broad. An excess of distances exists from 0.21 to 0.25 nm. The Zn–O coordination number found for the glass znt30 is ∼5.2 instead of 6 as given for the crystal. Also the number of Te–O distances in this r-range for the glass znt30 is obviously less than that of the crystal.

4.3. Short and long Te–O bonds and their relation to the TeO_4 and TeO_3 units

The subsequent paragraphs are aimed at examining further details about the TeO_n groups in the evolution of glass structure. The oxygen atoms in Te–O bonds of different lengths are considered. First, simple groups like those shown in figure 1 (introduction) are assumed: all bonds of TeO_3 units and the two short equatorial bonds of TeO_4 are related to N_{short} while the two longer axial bonds of TeO_4 units are related to N_{long}. Even longer bonds of TeO_{3+1} units are expected at ∼0.24 nm, which have not been taken into account in section 4.1. The dashed-curved peaks of the crystal structures (cf figure 9) at ∼0.19, ∼0.21 and ∼0.24 nm indicate the short Te–O bonds of TeO_4 and TeO_3 units, long Te–O bonds of TeO_4 units and even longer Te–O bonds of TeO_{3+1} units, respectively. Broadening due to structural disorder introduced by peak widths and truncation effects of FT cause a partial overlap of the three peaks. The

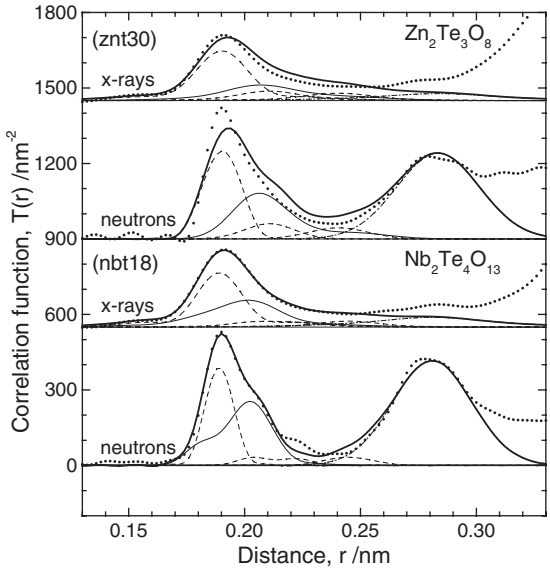

Figure 9. Comparison of the short-range order distances of binary tellurite glasses with 30 mol% ZnO or 18 mol% Nb_2O_5 with those of $Zn_2Te_3O_8$ [23] (40 mol% ZnO) and $Nb_2Te_4O_{13}$ [22] (20 mol% Nb_2O_5) crystals by means of the correlation functions $T_X(r)$ and $T_N(r)$. Experimental data, dotted curves; distances of the crystals, thick solid curves; peaks of the Te–O bonds of ∼0.19, ∼0.21 and ∼0.24 nm, dashed curves; peaks of Zn–O (or Nb–O) distances, thin solid curves.

crystal structure of $Nb_2Te_4O_{13}$ [22] with eight independent Te sites has a greater variety of distances than $Zn_2Te_3O_8$ [23] with two independent Te sites. This makes the crystal structure of $Nb_2Te_4O_{13}$ more useful for comparisons with a glass structure. Similar to fit results of the glasses (figure 6), the peak component at ∼0.19 nm is narrow while that at ∼0.21 nm is broad. Thus, fractions N_{short} and N_{long} belong to peak components being different in distance and in width. A greater problem is the overlap of the N_{long} fraction with the longer distances of TeO_{3+1} units. The borderline between both types of distance is located somewhere close to ∼0.235 nm. The fit results of N_{long} given in tables 2 and 3 might contain small contributions from the longer Te–O distances of TeO_{3+1} units. Therefore, in a next step, the N_3 are calculated from numbers N_{short}, remembering that TeO_3 and TeO_{3+1} units contribute with three Te–O bonds and TeO_4 units with two Te–O bonds. The fractions N_3 of TeO_3 (TeO_{3+1} included) are calculated from numbers N_{short} by $N_3 = N_{short} - 2$. Generally, the N_3 obtained in this way and shown in figures 10(a) and (b) behave similarly to those obtained from total N_{TeO} numbers ($N_{TeO} = N_{short} + N_{long}$) with $N_3 = 4 - N_{TeO}$ (cf figure 8). Some of the N_3 values do not change, while others change by ±0.1. Also the N_3 of the samples znt22 and nbt06 are found close to the model behaviour (all TeO_4 with NBO are transformed to TeO_3, see equation (2)). The N_3 of glasses of higher ZnO or Nb_2O_5 content tend to the N_3 of the related crystals, $Zn_2Te_3O_8$ [23] or $Nb_2Te_4O_{13}$ [22] respectively, which indicates similarity of structural features such as the existence of TeO_4 with NBO and, additionally, oxygen atoms in Nb–O–Nb bridges for the Nb tellurite glasses.

The similarity of the behaviour of N_3 calculated from numbers N_{TeO} or calculated from numbers N_{short} confirms the interpretation of the fractions N_{short} and N_{long} obtained in the fits. Thus, the fractions of groups obtained from total Te–O coordination numbers can be related to the expected polyhedra of TeO_3 and TeO_4 groups (trigonal pyramids and trigonal bipyramids). TeO_3 with three short and TeO_4 with two short and two long Te–O bonds co-exist in the

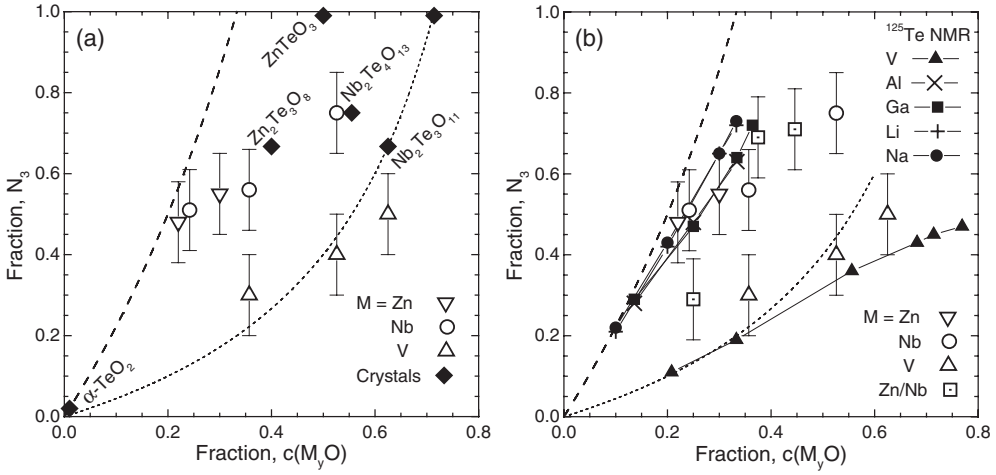

Figure 10. Fractions, N_3, of the TeO_3 units of the glasses studied versus fraction $c(M_yO)$ of modifier oxide. Here, different from figure 8, N_3-values are calculated from numbers of short Te–O bonds, N_{short}, assuming that a TeO_3 unit has three, a TeO_4 unit has two short bonds. Diffraction results are given with open symbols. Data of related crystal structures are indicated with solid diamonds (a). ^{125}Te NMR results [10, 12, 13] are plotted as solid symbols connected by curves (b). The dashed- and dotted-curved functions give specific models of modifier behaviour which are explained in the text.

structures. The transition from TeO_4 to TeO_3 groups [9–12] gives a plausible explanation of the structural evolution. The role of TeO_{3+1} units as part of the TeO_3 fraction is not clarified by our experiments. Determination of the contributions of Te–O bonds with lengths of more than ∼0.24 nm is outside the r-range of our fits.

4.4. Arguments for the existence of well-defined TeO_4 and TeO_3 units

It is argued [45] that TeO_n polyhedra can be distorted easily because the lone pair of electrons together with the four or three oxygen atoms of TeO_4 or TeO_3 units form polyhedra of low symmetry. Quantification of these distortions is difficult. Differentiation of TeO_4, TeO_3 or TeO_{3+1} units is sometimes made on the basis of diffraction data of poor resolving power as was also done for a ZnO–TeO_2 glass [45]. The qualitative considerations, however, were based on comparisons with related crystal structures. A similar situation exists for EXAFS results. A Te–K EXAFS study of Nb tellurite glasses [46] reported co-existence of TeO_4 and TeO_{3+1} units, but TeO_3 units were excluded from the fits. In the $Nb_2Te_4O_{13}$ [22] crystal, for example, four of six TeO_3 groups have a fourth longer Te–O bond and can be called a TeO_{3+1} group. The corresponding longer Te–O distances are found between 0.235 and 0.255 nm where fits of our $T_N(r)$ and $T_X(r)$ data free of arbitrariness are not possible. Before we continue with the discussion of the distortions of groups and their possible transitional states two other plots are presented. Figure 11(a) shows the numbers N_{short} and N_{long} as a function of N_{TeO}. N_{TeO} ranges from four (only TeO_4) to three (only TeO_3 units). Straight lines indicate the expected fractions of short and long Te–O bonds for a behaviour where a TeO_3 has three short bonds and a TeO_4 has two short and two long bonds. The corresponding numbers of three crystal structures are also given. Above, numbers N_{short} have been used for calculation of N_3 fractions, a method which avoids the problems of overlap of the long Te–O bonds of TeO_4 units (N_{long}) with the longer bonds of TeO_{3+1} units (cf results in figure 10). Figure 11(b) shows total N_{TeO}

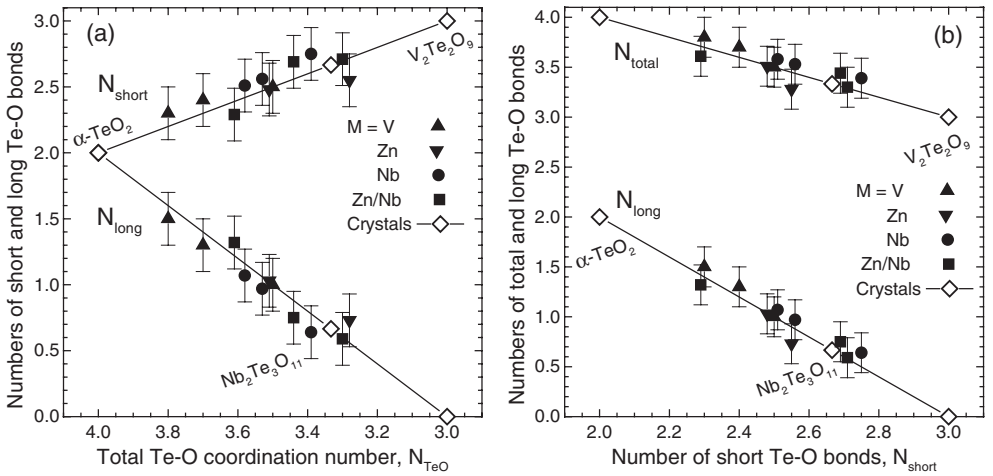

Figure 11. Behaviour of the numbers N_{short} and N_{long} in dependence on their sum N_{TeO} (a) and behaviour of the numbers N_{TeO} and N_{long} in dependence on N_{short} (b) of the glasses of the present study and of V tellurite glasses [14]. Straight lines indicate the behaviour expected for existence of TeO_4 trigonal bipyramids and TeO_3 trigonal pyramids where also numbers of the crystal structures lying on the dotted curve in figures 8 and 10 are given.

and N_{long} as a function of N_{short} following this idea. Different effects of the second oxide on the $TeO_4 \rightarrow TeO_3$ transition in the tellurite networks are neglected in figures 11(a) and (b). The figures demonstrate that experimental numbers N_{short} and N_{long} follow the lines for co-existence of well-defined TeO_4 and TeO_3 groups. The small deviations are in the limits of uncertainty of the fits. They do not show any other trend than that predicted. Figure 11(b) is more suitable than 11(a) for estimation of the effects of uncertain N_{long} numbers. The deviations of N_{long} from the straight line in figure 11(b) can be interpreted easily: all numbers above the lines indicate N_{long} is too high in relation to the corresponding N_{short} and vice versa. More of the numbers N_{long} are too high by $\sim$0.1, which can be explained by contributions from some TeO_{3+1} units having a fourth Te–O bond of length less than 0.240 nm.

In principal, diffraction results of disordered structures are not capable of identifying the bonds which belong to individual structural units but average numbers of pair distances are obtained. From knowledge of the total N_{TeO} numbers we cannot conclude absence of groups showing all geometrical varieties between TeO_4 and TeO_{3+1} or TeO_3 units as they are discussed in [46]. But the resulting behaviour of the numbers N_{short} and N_{long} of the modified tellurite glasses studied indicates the existence of mostly well-defined TeO_4 and TeO_3 (TeO_{3+1}) units instead of their transitional states. All distances of N_{long} belong to TeO_4 groups and indicate their fraction. Not accepting this behaviour would have the following consequences: supposing TeO_4 units exist with three short bonds but only one bond belonging to N_{long}. Such a TeO_4^* group would be similar to a TeO_{3+1} unit but with a relatively short fourth bond. According to the behaviour found for N_{short} and N_{long} (figure 11) the occurrence of such a TeO_4^* unit would have to be compensated by a TeO_3^* unit with only two short Te–O bonds and a single longer bond. Such TeO_4^* and TeO_3^* units differing in the number of short bonds but equal in the number of long bonds (i.e. one) are not known. Their stability is quite questionable. A relation of bond valency (BV) and bond length (R) is given by Philippot [47] with $\text{BV} = 1.333(R/0.1854)^{-5.2}$ (R in nanometres). The sum of the BV of a Te site should be close to 4. The BV values are 1.2, 0.7 and 0.35 for Te–O distances of 0.189, 0.21 and 0.24 nm respectively. If the sum of BV of a TeO_3 unit is calculated according to distances of the short Te–O bonds found with

0.189 nm (tables 2, 3), an additional bond of a length of ∼0.24 nm is useful to complete the sum of BV to 4. This polyhedron is the typical TeO_{3+1} unit. A shorter fourth bond, such as assumed for TeO_4^* units, makes the sum of BV greater than 4. On the other hand, the sum of BV of the TeO_3^* unit of two short and one long third Te–O bond is clearly less than 4.

Thus, well-defined groups like those shown in figure 1 for α-TeO_2 [18], β-TeO_2 [19], $Nb_2Te_3O_{11}$ [21] or $Zn_2Te_3O_8$ [23] crystals are suggested to form the glass structures. The TeO_4 unit of $Nb_2Te_4O_{13}$ [22] is already more distorted, with both axial bonds differing by 0.02 nm. The TeO_4 group shown for γ-TeO_2 [20] does not allow a differentiation into short and long Te–O bonds. It is still identified as a trigonal bipyramid although it shows tendencies of transition to a TeO_{3+1} unit. Stronger distortions of the TeO_4 groups are also reported in an *ab initio* molecular orbital (MO) study of a small cluster model of TeO_2 glass [17]. The first-neighbour peak in the radial distribution from diffraction data of glassy TeO_2 [17] shows a sharp component at ∼0.19 nm but a clear differentiation of two short and two long Te–O bonds does not seem to be possible for the TeO_4 units of this glass. It is remembered that TeO_2 is difficult to obtain in glassy form. Well-defined TeO_4 groups with two short and two long bonds are only obtained with asymmetric Te–O–Te bridges where, as found in α-TeO_2 [18], a short equatorial and a long axial Te–O bond participate. This is difficult to realize in fully connected but disordered TeO_2 networks. On the other hand, mixtures of TeO_4 and TeO_3 groups accompanied by numerous NBO in modified tellurite networks reduce the stress to the internal geometry of groups. Another *ab initio* MO calculation of clusters is made for $Te_2O_5^{2-}$ and Na^+ ions [17]. Here the transition of TeO_4 to TeO_3 units is already finished, and TeO_{3+1} and TeO_3 units co-exist.

Modelling should clarify further features of connections of groups and of stacking of the tellurite network units with the oxygen polyhedra of the second oxide. For example, the reverse Monte Carlo method was applied to model structures of Na tellurite glasses [48], but modelling of tellurite structures is difficult. Inappropriate geometries of the structural units are obtained if the lone pair of electrons of Te atoms is neglected. Most crystal structures are not suitable for giving an idea of the three-dimensional arrangement of the structural elements. The structure of the above-discussed $Nb_2Te_4O_{13}$ [22] crystal is formed of stacked layers which are alternatively occupied by NbO_6 octahedra, TeO_3 units and short tellurite chains, a structure which is hard to accept for a glass.

4.5. Structural groups of mixed Zn/Nb tellurite glasses

The determination of Te–O coordination numbers of the ternary Zn/Nb tellurite glasses is of limited accuracy because distributions of Zn–O and Nb–O distances had to be fixed in the fits. However, the results given in figures 8(b), 10(b) and 11 show that N_{TeO}, N_{short} and N_{long} do not behave differently from those of the binary glasses. The N_3 values of the ternary glasses are calculated assuming that modifying effects of both oxides can be added. The effect of ZnO additions is calculated according to equation (2) and the effect of Nb_2O_5 additions is determined according to that of samples nbt06 and nbt10. The calculated N_3 fractions for samples nzt05, nzt20 and nzt12 are 0.41, 0.72 and 0.70 while the N_3 obtained from the fits are 0.39, 0.56 and 0.70 respectively. Also N_3-fractions are calculated from numbers N_{short} with results in 0.29, 0.69 and 0.71. The two differing numbers can be due to the disadvantage of fixed parameters for the Zn–O and Nb–O peaks in the fits. But in limits of uncertainty, the agreement of the other N_3 demonstrates the additivity of the effects of ZnO and Nb_2O_5 additions. Unfortunately, we did not measure a ternary sample of higher Nb_2O_5 content. N_3 fractions higher than those obtained for the binary glasses become possible. Note that the limit of glass formation of the binary systems is found with $Zn_2Te_3O_8$ [23] and $Nb_2Te_4O_{13}$ [22] crystals.

5. Conclusions

Combinations of neutron and x-ray diffraction data allow the Te–O and Zn–O (or Nb–O) correlations to be resolved in the range of the first-neighbour peaks of binary tellurite glasses. Moreover, the high resolving power of the neutron experiments with Q_{max} of 400 nm^{-1} allows the determination of components of short Te–O bonds with a narrow distribution of lengths centred at ∼0.188 nm and long Te–O bonds with a broad distribution of lengths centred at ∼0.210 nm. The Te–O coordination numbers, N_{TeO}, of the glasses studied range from 3.3 to 3.6; the N_{TeO} values of Zn tellurite glasses show the behaviour of a typical modifying oxide while the N_{TeO} values of Nb tellurite glasses indicate a change from network-modifying to network-forming behaviour with increasing Nb_2O_5 content.

Changes of N_{TeO}, as well as of N_{short} and N_{long}, are interpreted as follows: if a second oxide is added to TeO_2 networks formed from corner-connected TeO_4 units, the modification process starts with rupture of Te–O–Te bridges and change of the two participating TeO_4 to TeO_3 units, each of latter having two NBO. Among the samples studied only that with 22 mol% ZnO shows this behaviour. Further increasing the modifier content stabilizes TeO_4 units with NBO. Finally, some O atoms are found in Nb–O–Nb bridges in the case of Nb tellurite glasses. The resulting parameters N_{TeO}, N_{short}, N_{long} for Te–O distances up to 0.24 nm are interpreted as TeO_4 trigonal bipyramids (two short equatorial and two long axial bonds) and TeO_3 trigonal pyramids (three short bonds). The longer distances of possibly existing TeO_{3+1} units are outside the r-range of a reliable fit and so the TeO_{3+1} are members of the TeO_3 fractions. Transitional forms between TeO_4 and TeO_{3+1} play a negligible role.

The N_{TeO} obtained for ternary Zn/Nb tellurite glasses agree with those calculated by summing up the effects of the participating ZnO and Nb_2O_5 additions.

References

[1] Vogel W, Bürger H, Müller B, Zerge G, Müller W and Forkel K 1974 *Silikattechnik* **25** 205
[2] Vogel E M, Weber M J and Krol D M 1991 *Phys. Chem. Glasses* **32** 231
[3] El-Mallawany R 2002 *Tellurite Glasses Handbook, Physical Properties and Data* (Boca Raton, FL: CRC Press)
[4] Kim S-H and Yoko T 1995 *J. Am. Ceram. Soc.* **78** 1061
[5] Shen S X, Jha A, Liu X B, Naftaly M, Bindra K, Bookey H J and Kar A K 2002 *J. Am. Ceram. Soc.* **85** 1391
[6] Tokuda Y, Saito M, Takahashi M, Yamada K, Watanabe W, Itoh K and Yoko T 2003 *J. Non-Cryst. Solids* **326/327** 472
[7] Mochida N, Takahashi K, Nakata K and Shibusawa S 1978 *Yogyo-Kyokai-Shi* **86** 316
[8] Dimitriev Y, Dimitrov V and Arnaudov M 1983 *J. Mater. Sci.* **18** 1353
[9] Himei Y, Osaka A, Nanba T and Miura Y 1994 *J. Non-Cryst. Solids* **177** 164
[10] Sakida S, Hayakawa S and Yoko T 1999 *J. Non-Cryst. Solids* **243** 13
[11] Sakida S, Hayakawa S and Yoko T 1999 *J. Ceram. Soc. Japan* **107** 395
[12] Sakida S, Hayakawa S and Yoko T 2001 *J. Am. Ceram. Soc.* **84** 836
[13] Sakida S, Hayakawa S and Yoko T 2000 *J. Phys.: Condens. Matter* **12** 2579
[14] Hoppe U, Yousef E, Rüssel C, Neuefeind J and Hannon A C 2002 *Solid State Commun.* **123** 273
[15] Ueno M and Suzuki K 1983 *Res. Rep. Lab. Nucl. Sci. Tohoku Univ.* **16** 49
[16] Suzuki K 1987 *J. Non-Cryst. Solids* **95–96** 15
[17] Niida H, Uchino T, Jin J, Kim S-H, Fukunaga T and Yoko T 2001 *J. Chem. Phys.* **114** 459
[18] Lindquist O 1968 *Acta Chem. Scand.* **22** 977
[19] Beyer H 1967 *Z. Kristallogr.* **124** 228
[20] Champarnaud-Mesjard J-C, Blanchandin S, Thomas P, Mirgorodsky A P, Merle-Méjean T and Frit B 2000 *J. Phys. Chem. Solids* **61** 1499
[21] Galy J and Lindquist O 1979 *J. Solid State Chem.* **27** 279
[22] Blanchandin S, Champarnaud-Mesjard J C, Thomas P and Frit B 2000 *J. Alloys Compounds* **306** 175
[23] Hanke K 1966 *Naturwissenschaften* **53** 273
[24] Loopstra B O and Goubitz K 1986 *Acta Crystallogr.* C **42** 520

[25] Bürger H, Kneipp K, Hobert H, Vogel W, Kozhukharov V and Neov S 1992 *J. Non-Cryst. Solids* **151** 134
[26] Sekiya T, Mochida N, Ohtsuka A and Tonokawa M 1992 *J. Non-Cryst. Solids* **144** 128
[27] Sekiya T, Mochida N and Ohtsuka A 1994 *J. Non-Cryst. Solids* **168** 106
[28] Berthereau A, Le Luyer Y, Olazcuaga R, Le Flem G, Couzi M, Canioni L, Segonds P, Sarger L and Ducasse A 1994 *Mater. Res. Bull.* **29** 933
[29] Hannon A C, Howells W S and Soper A K 1990 *Inst. Phys. Conf. Ser.* **107** 193
[30] Faber T E and Ziman J M 1965 *Phil. Mag.* **11** 153
[31] Poulsen H F, Neuefeind J, Neumann H-B, Schneider J R and Zeidler M D 1995 *J. Non-Cryst. Solids* **188** 63
[32] Waasmeier D and Kirfel A 1995 *Acta Crystallogr.* A **51** 416
[33] Maslen E N, Fox A G and O'Keefe M A 1992 *International Tables for Crystallography* vol C, ed A J C Wilson (Dordrecht: Kluwer) p 476
[34] Hubbell J H, Veigele Wm J, Briggs E A, Brown R T, Cromer D T and Howerton R J 1975 *J. Phys. Chem. Ref. Data* **4** 471
[35] Waseda Y 1980 *The Structure of Non-Crystalline Materials* (New York: McGraw-Hill) p 11
[36] Lorch E A 1969 *J. Phys. C: Solid State Phys.* **2** 229
[37] Wright A C and Leadbetter A J 1976 *Phys. Chem. Glasses* **17** 122
[38] Mozzi R L and Warren B E 1969 *J. Appl. Crystallogr.* **2** 164
[39] Leadbetter A J and Wright A C 1972 *J. Non-Cryst. Solids* **7** 23
[40] Marquardt D 1963 *SIAM J. Appl. Math.* **11** 431
[41] Hoppe U, Kranold R, Barz A, Stachel D, Neuefeind J and Keen D A 2001 *J. Non-Cryst. Solids* **293–295** 158
[42] Hoppe U, Kranold R, Gattef E, Neuefeind J and Keen D A 2001 *Z. Naturf.* a **56** 478
[43] Hanke K 1967 *Naturwissenschaften* **54** 199
[44] Darriet J and Galy J 1973 *Cryst. Struct. Commun.* **2** 237
[45] Kozhukharov V, Bürger H, Neov S and Sidzhimov B 1986 *Polyhedron* **5** 771
[46] Berthereau A, Fargin E, Villezusanne A, Olazcuaga R, Le Flem G and Ducasse L 1996 *J. Solid State Chem.* **126** 143
[47] Philippot E 1981 *J. Solid State Chem.* **38** 26
[48] McLaughlin J C, Tagg S L, Zwanziger J W, Haeffner D R and Shastri S D 2000 *J. Non-Cryst. Solids* **274** 1